

Revealing the complex nature of bonding in binary high-pressure compound FeO₂

E. Koemets,^{1,2} I. Leonov,^{3,4,5} M. Bykov,¹ E. Bykova,^{1,6} S. Chariton,¹ G. Aprilis,^{7,8} T. Fedotenko,⁷ S. Clément,⁹ J. Rouquette,² J. Haines,² V. Cerantola,⁸ K. Glazyrin,¹⁰ C. McCammon,¹ V. B. Prakapenka,¹¹ M. Hanfland,⁸ H.-P. Liermann,¹⁰ V. Svitlyk,⁸ R. Torchio,⁸ A. D. Rosa,⁸ T. Irifune,¹² A. V. Ponomareva,⁴ I. A. Abrikosov,¹³ N. Dubrovinskaia,^{7,13} and L. Dubrovinsky¹

¹*Bayerisches Geoinstitut, University of Bayreuth, D-95440 Bayreuth, Germany*

²*Institut Charles Gerhardt Montpellier (UMR CNRS 5253),*

Université de Montpellier, F-34095, Montpellier cedex 5, France

³*Institute of Metal Physics, Sofia Kovalevskaya Street 18, 620219 Yekaterinburg GSP-170, Russia*

⁴*Materials Modeling and Development Laboratory, NUST "MISIS", 119049 Moscow, Russia*

⁵*Ural Federal University, 620002 Yekaterinburg, Russia*

⁶*Carnegie Institution of Washington, Earth and Planets Laboratory,*

5241 Broad Branch Road, N.W., Washington, DC, 20015, USA

⁷*Material Physics and Technology at Extreme Conditions,*

Laboratory of Crystallography, Universität Bayreuth, D-95440 Bayreuth, Germany

⁸*The European Synchrotron Radiation Facility, 38043 Grenoble Cedex 9, France*

⁹*Laboratoire Charles Coulomb (L2C) - UMR CNRS 5221 Université de Montpellier. CC069, 34095 Montpellier, France*

¹⁰*Photon Science, Deutsches Elektronen-Synchrotron, D-22607 Hamburg, Germany*

¹¹*Center for Advanced Radiation Sources, University of Chicago, Chicago, Illinois 60437, USA*

¹²*Geodynamics Research Center, Ehime University, 2-5 Bunkyo-cho, Matsuyama 790-8577, Japan*

¹³*Department of Physics, Chemistry and Biology (IFM),*

Linköping University, SE-581 83 Linköping, Sweden

Extreme pressures and temperatures are known to drastically affect the chemistry of iron oxides resulting in numerous compounds forming homologous series $n\text{FeO}\cdot m\text{Fe}_2\text{O}_3$ and the appearance of FeO₂. Here, based on the results of *in situ* single-crystal X-ray diffraction, Mössbauer spectroscopy, X-ray absorption spectroscopy, and DFT+dynamical mean-field theory calculations we demonstrate that iron in high pressure cubic FeO₂ and isostructural FeO₂H_{0.5} is ferric (Fe³⁺), and oxygen has a formal valence less than two. Reduction of oxygen valence from 2, common for oxides, down to 1.5 can be explained by a formation of a localized hole at oxygen sites.

At ambient (or low) pressures, three different iron oxides are known: Fe₂O₃ with a mineral name hematite; Fe₃O₄ magnetite – the oldest known magnetic material, and FeO wüstite, which is non-stoichiometric and typically iron deficient. At extreme pressures and temperatures, the synthesis yields numerous iron oxides with unexpected compositions (such as Fe₄O₅, Fe₅O₆, Fe₇O₉, Fe₅O₇, Fe₂₅O₃₂, etc.), unusual crystal structures, and intriguing physical properties, demonstrating the complexity of the binary Fe-O system [1–5]. It was suggested that iron oxides at high-pressure and high-temperature conditions (HP-HT) could be systematized by homologous structural series $n\text{FeO}\cdot m\text{Fe}_2\text{O}_3$ formed by oxygen (O²⁻) and iron in ferrous and/or ferric states (Fe²⁺ and Fe³⁺, correspondingly). Besides the end-members, iron could exist in the mixed-valence state in this series (intermediate between 2+ and 3+ valence formally), defined by the stoichiometry of HP iron oxides. However, the recent finding of cubic FeO₂ (space group $Pa\bar{3}$), and closely related FeO₂H_{*x*} (*x* up to 1) phases [7–9] suggests that not only iron but also oxygen could have a variable oxidation state in iron oxides (or oxyhydroxides).

Powder X-ray diffraction (PXRD) [7], X-ray Absorption Spectroscopy (XAS, [10, 11]), and Nuclear Forward Scattering (NFS) studies [11] of cubic high-pressure

FeO₂H_{*x*} (*x* = 0 to 1) compounds as well as results of some theoretical works [12, 13] were used to argue that iron is ferrous in these phases even at strongly oxidized conditions and thus oxygen forms peroxide (O₂)²⁻ ions. However, the question concerning the oxidation state of both iron and oxygen in FeO₂ and FeO₂H_{*x*} remains controversial, primarily because of harsh experimental conditions and ambiguous results. For example, while XAS data were interpreted to indicate that iron is ferrous [10, 11], yet NFS data of cubic FeO₂ [11] shows center shifts (~0.15 mm/s at 80 GPa) that are unrealistic for any ferrous compound. The HP-HT synthesis of the FeO₂H_{*x*} phase for the XAS analysis in the work [10] was performed from FeOOH using KCl as a pressure transmitting medium, which could chemically react [14] and the reaction products could affect interpretation of spectra collected for FeO₂H_{*x*} phase. Available experimental information on the crystal structure of FeO₂ and FeO₂H_{*x*} phases is based on PXRD [7, 9], which makes the analysis of the Fe-O and O-O distances unreliable compared to more complex yet more informative structural refinements from single-crystal X-ray diffraction data (SC-XRD) [15]. Additionally, some theoretical works [16–19] suggest that iron is ferric in FeO₂ illustrating the necessity of performing high-accuracy exper-

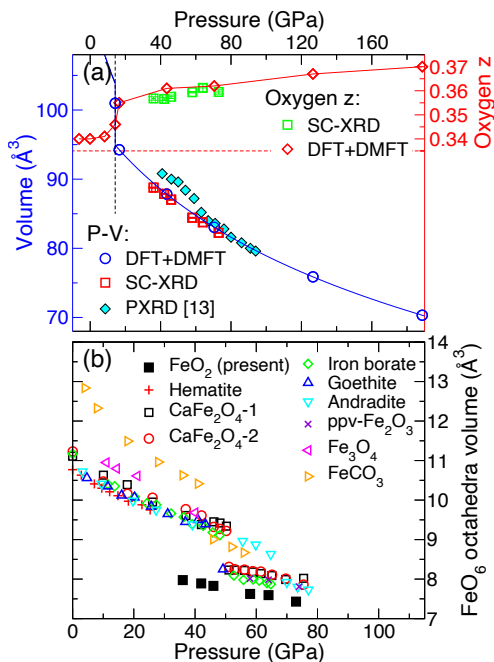


FIG. 1: (Color online) Compressional behavior of HP-PdF₂-type FeO₂: (a) lattice volume and fractional z coordinate of oxygen under pressure as obtained by DFT+DMFT at $T = 1160$ K in comparison to XRD data. Note that below ~ 14 GPa, FeO₂ shows a low-spin to high-spin phase transition, associated with the formation of local moments. (b) Pressure dependence of volumes of the FeO₆ octahedra in various compounds according to Ref. [32] and references therein.

iments to establish the physical and chemical properties of this phase.

The goals of the present work are to clarify the high-pressure crystal chemistry of cubic FeO₂ and FeO₂H _{x} phases and determine the oxidation state of iron and oxygen. These are not only of importance as a fundamental problem for HP-HT chemistry but also highly relevant for geosciences [7]. In order to achieve the goals of our studies, we perform multi-method synchrotron-based experiments including advanced *in situ* SC-XRD, X-ray absorption and Mössbauer spectroscopy using laser-heated diamond anvil cells (see Supplementary Material [6], Table S1). We support our experimental results by the DFT+dynamical mean-field theory (DFT+DMFT) calculations [20, 21] of the electronic structure, magnetic and valence state of iron. In addition, we perform a full structural optimization and compute the crystal structure parameters of paramagnetic FeO₂ under pressure within DFT+DMFT [22–28]. Our experimental and theoretical results suggest that iron in HP-PdF₂-type FeO₂ and FeO₂H _{x} is ferric (3+). We show the absence of a molecular (O₂)³⁻ bonding state in HP-PdF₂-type FeO₂, implying that the oxidation state of oxygen is equal to 1.5- due to oxygen-metal negative charge transfer. Such a charge transfer is expected to shorten the Fe-O distance

and consequently reduce the volume of FeO₆ octahedra, which should cause both iron polyhedra and the entire structure to become highly incompressible. We propose that in major phases constituting the lower mantle and the core-mantle boundary the oxidation state of oxygen may significantly deviate from 2- due to this effect.

Compression of iron in oxygen at ambient temperature to 25(1) GPa did not produce any chemical reaction, but laser heating of the sample at this pressure to $\sim 1500(100)$ K led to the formation of Fe₂O₃ (space group $R\bar{3}c$, lattice parameters $a = 6.271(7)$ Å, $c = 7.662(4)$ Å) (see Fig. S2), in agreement with literature data [29]. After further compression to 46(2) GPa, the laser heating of a sample was performed at $\sim 1200(100)$ K. The XRD pattern of the temperature-quenched product drastically changed. The XRD analysis shows cubic FeO₂ with the space group $Pa\bar{3}$ and unit cell parameter $a = 4.4313(14)$ Å, which is close to the values previously reported for “pyrite-type” FeO₂ [7, 18]. Iterative heating of the samples at different pressures resulted in the growth of micro-crystals of cubic FeO₂ that enabled performing an *in situ* SC-XRD data collection, the structure solution, and further refinements with the HP-PdF₂-type structure in a range of pressures from 36(1) to 73(2) GPa, (see Table S1[6]). The results on the crystal structure refinements from *in situ* SC-XRD datasets of the FeO₂, which have never been reported before, are summarized in Table S2[6]; the illustration of corresponding crystal structure of HP-PdF₂ FeO₂ is presented in Fig. S1[6]; the compressional behavior of this phase is presented in Fig. 1. Structural analysis suggests that the shortest O-O bond length (in the O-O dimer) varies from 2.213(7) to 2.104(15) Å within the pressure range from ~ 36 to 73 GPa (see Table S2). For peroxides (in molecular or crystalline forms), the distances between the closest oxygen atoms at ambient pressure are very characteristic – from about 1.2 to 1.5 Å [30] (e.g., in MgO₂ it is about 1.492 Å at ambient pressure) and under compression these distances should not increase. In the case of FeO₂, such a large observed value for the shortest O-O distance suggests, from crystal-chemical point of view, the absence of chemical bonding between these oxygen atoms. Even in the case of the structural model of FeO₂ refined against powder XRD data (“pyrite-type FeO₂” model [7]), the shortest O-O bond is ~ 1.896 Å at 76 GPa which is too large for peroxides.

A number of transition metals, for example, osmium and ruthenium, the neighbors of iron in the VIIIb group of the Periodic Table, form dioxides, OsO₂ and RuO₂ with the HP-PdF₂-type structure [31, 32] (space group $Pa\bar{3}$). The shortest O-O distance in these dioxides is equal to ~ 2.5 Å at ambient conditions. These phases are characterized by low compressibility (for details see Refs. [31, 32]), and cubic FeO₂ is very incompressible as well, according to our experimental data (see Fig. 1(b)). Thus, accounting for the relatively long O-O distances

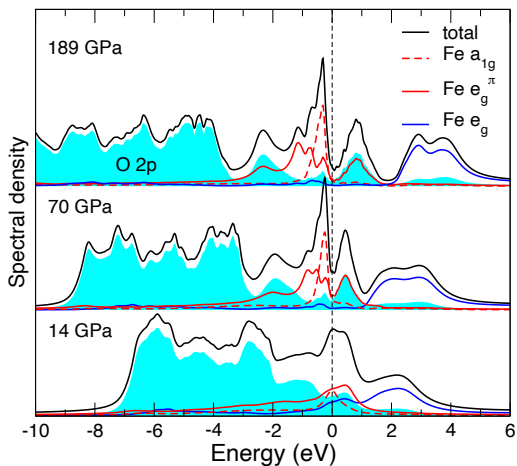


FIG. 2: (Color online) Orbitaly-resolved spectral functions of HP-PdF₂-type FeO₂ for the Fe 3d (a_{1g} , e_g^π and e_g^σ) and O 2p (blue shaded area) states obtained by DFT+DMFT at 1160 K as a function of compression.

in FeO₂ at HP, one could expect that it adopts rather the HP-PdF₂-type structure than forms a peroxide. Additionally, according to the “rule of a thumb” [33], the behavior of compounds (particularly oxides) of an element at high pressure is similar to that of compounds of the elements with higher atomic number in the same group of the Periodic Table at low pressures.

The results of structural studies and crystal-chemical considerations are consistent and pointing towards highly unusual crystal chemistry of Fe-O bonds in HP-PdF₂-type FeO₂. In fact, Streltsov *et al.* [16] have suggested on the basis of *ab initio* calculations for FeO₂ that the valence of iron is 3+ and have classified the material as lying “in between” oxides and peroxides with the anion described as (O₂)³⁻. However, the structural model obtained from the powder diffraction analysis reported by Hu *et al.* [7] have been used in the calculations, and the input crystal structure of cubic FeO₂ has not been optimized self-consistently [16]. While other electronic structure studies used the DFT+U method to compute the crystal structure parameters of FeO₂ [12, 13, 19], these computations assume the existence of a long-range magnetic order in HP-PdF₂ phase of FeO₂, in contradiction with experiment. As a result, such computations cannot give a reliable results for the shortest O-O bond length in FeO₂, predicting either a highly unusual increase of the O-O distance under pressure [12] or a large O-O distance of 2.232 Å at 76 GPa [19].

We resolve this point by computing the crystal structure phase stability and electronic structure of the paramagnetic HP-PdF₂ phase of FeO₂ using a fully charge self-consistent DFT+DMFT method (see Suppl. Material [6]). Within DFT+DMFT we perform a full structural optimization of the lattice parameters of the *paramagnetic* HP-PdF₂ phase of FeO₂ and compare our results

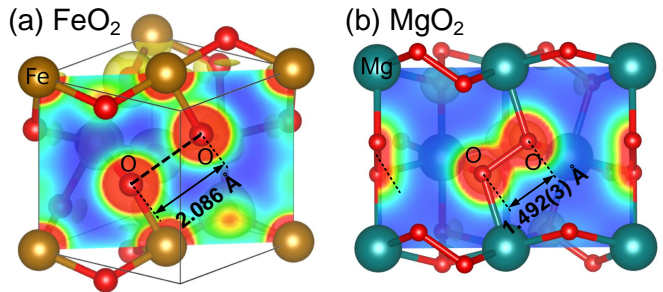


FIG. 3: (Color online) (a) Crystal structure and valence electron density plot for HP-PdF₂-type FeO₂ obtained by DFT+DMFT at $T = 1160$ K and 70 GPa (unit cell volume 83.0 Å³, the calculated O-O distance 2.086 Å is too large for the peroxide-type structure). (b) DFT (HSE03) results for pyrite-type MgO₂ peroxide at ambient conditions (uni cell volume 113.3 Å³ and the O-O distance is about 1.492(3) Å [41]).

with experimental data obtained through more precise *in situ* SC-XRD. In Fig. 1 we display our results for the crystal structure parameters obtained by DFT+DMFT. In contrast to the previous DFT+U results [12], we observe that upon compression the O-O distance decreases from 2.286 Å at 17 GPa to 2.085 Å at 70 GPa, which is in close agreement with our SC-XRD data. Indeed, our SC-XRD measurements give $\sim 2.213(7)$ Å at 36(1) GPa and 2.117(8) Å at 73(2) GPa. Our DFT+DMFT calculations show that at a pressure of ~ 70 GPa FeO₂ is a poor metal (see Fig. 2) with about 5.21 electrons in the Wannier Fe 3d states (4.07 electrons inside the atomic sphere with radius ~ 0.78 Å, in accord with a bond valence analysis). Oxygen states are partially occupied with ~ 0.61 hole states in the Wannier O 2p orbitals. The local magnetic moment is $\sim 1.59 \mu_B$ (fluctuating local moment of 0.83 μ_B). Our results for the decomposition of electronic state into atomic configurations (valence states) show that the valence value for Fe is nearly 3+ at ~ 70 GPa: Fe³⁺ 3d⁵ configuration has a weight of about 50%, with a $\sim 30\%$ admixture of the Fe²⁺ 3d⁶ state ($\sqrt{0.5}|d^5\rangle + \sqrt{0.3}|d^6\rangle$), see Fig. S7).

In Fig. 2 we see that due to distorted FeO₆ octahedron symmetry, the Fe t_{2g} states split into a a_{1g} singlet and e_g^π doublet. Fe e_g^σ orbitals are empty and are located well above the Fermi level at 1–4 eV. Fe t_{2g} states form weakly renormalized ($m/m^* \sim 1.6$) quasiparticle bands near E_F . No evidence for a metal-to-insulator phase transition in FeO₂ (below ~ 189 GPa) was observed within our fully relaxed DFT+DMFT calculations [12, 13], in agreement with experiment. In fact, under experimental setup presented here samples were black with a metallic shine, implying a metallic state of FeO₂. Moreover, within DFT+DMFT the low-to-high spin state transition is found to occur below ~ 14 GPa, i.e., below the stability field of the HP-PdF₂-type FeO₂. We therefore propose

that decomposition of FeO_2 experimentally observed below ~ 30 GPa is associated with a change of the electronic state of iron in FeO_2 . Most notably, our DFT+DMFT results confirm that even at ~ 189 GPa the shortest O-O bond remains sufficiently large (1.86 \AA), implying the absence of covalent “molecular” O-O bonding in FeO_2 .

The DFT+DMFT results agree well with our Mössbauer and X-ray absorption spectroscopy data that shows a low-spin state of nearly $3+$ iron ions in the studied pressure range (see below). Most importantly, our fully relaxed and charge self-consistent DFT+DMFT calculations lead to a different bonding picture of FeO_2 in comparison to the analysis by Streltsov *et al.* [16]. Our results reveal the absence of a molecular $(\text{O}_2)^{3-}$ bonding state, i.e., in FeO_2 iron has effective charge $3+$, and oxygen $1.5-$. We see that at about 70 GPa the bonding O-O σ states appear at about -2 eV, while the anti-bonding σ^* states due to mixing with the Fe t_{2g} states at the Fermi level split into the $t_{2g} \pm \sigma^*$ combinations (seen as two peaks at -0.5 and $+0.5$ eV). Importantly, the empty $t_{2g} - \sigma^*$ O-O band is located ~ 0.5 eV above the Fermi level, confirming the formation of a localized hole at the O sites. We conclude that FeO_2 belongs to the class of negative charge-transfer materials in the Zaanen-Sawatzky-Allen scheme (materials in which excitation energy for the transfer of electrons from the O $2p$ to Fe $3d$ states is negative) [34, 35]. In such materials, instead of having an electronic configuration corresponding to the formal valence state, e.g. Fe^{4+} ($3d^4$) and O^{2-} ($2p^6$) configuration in FeO_2 , the system prefers to have a configuration with higher occupation of the $3d$ -shell, creating holes on oxygen.

At the same time, the bonding-antibonding splitting of the O $2p$ orbitals is small, just $\sim 2-3$ eV, indicating negligible bonding between the two oxygen atoms. This agrees well with our analysis of the charge density distribution in FeO_2 in comparison to magnesium peroxide MgO_2 (space group $Pa\bar{3}$). Our results are summarized in Fig. 3, highlighting the conclusion regarding the absence of a molecular $(\text{O}_2)^{3-}$ or $(\text{O}_2)^{2-}$ bonding state in FeO_2 in the studied interval of pressures. In fact, while MgO_2 clearly shows the formation of a “molecular” $(\text{O}_2)^{2-}$ bond with $\sim 21\%$ of a maximal electron density value in the center of the O-O bond, for cubic FeO_2 the value is only 5% at 70 GPa (it increases to $\sim 8\%$ at 189 GPa, see Fig. S7). Thus, in sharp contrast to MgO_2 no covalent O-O bond is seen for FeO_2 in Fig. 3. Therefore, the results of explicit examination of the calculated electronic structure and charge density distribution in HP-PdF₂-type FeO_2 confirms our above conclusion on the absence of chemical bonding between these oxygen atoms, as well as that Fe oxidation state is nearly $3+$.

Our Mössbauer spectroscopy data (see Fig. S4) are consistent with iron in the Fe^{3+} state [3, 36]. We note that the center shift that we obtained for cubic FeO_2 at 58(2) GPa ($0.06(5)$ mm/s) is in good agreement with

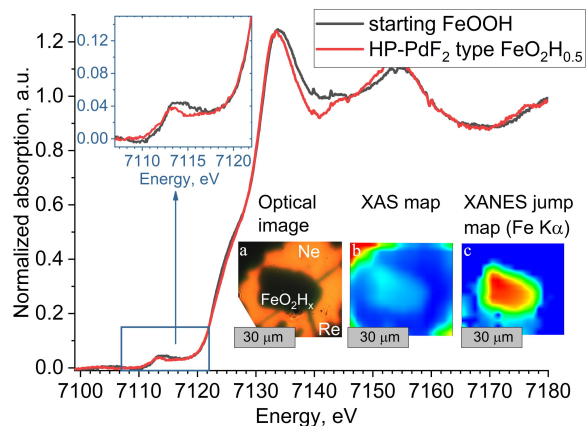


FIG. 4: (Color online) Normalized X-ray absorption spectra of Fe $K\alpha$ edge for $\text{FeO}_2\text{H}_{0.5}$ at 86(2) GPa (red line) synthesized from starting FeOOH (gray line) after laser-heating to 1700(200)K at 86(2) GPa (DAC11, see Table S1). Bottom right inset: (a) Microphotograph of synthesized $\text{FeO}_2\text{H}_{0.5}$ sample; (b) and (c) XAS absorption contrast and absorption jump maps of sample chamber (data collected with steps of $3 \mu\text{m}$ covering the whole sample chamber, palette reflects the relative values of the absorption and absorption jump).

the value of Liu *et al.* [11]. Our experimental and theoretical results thus imply that the oxidation state of oxygen in HP-PdF₂-type FeO_2 is equal to $1.5-$ due to oxygen-metal negative charge transfer. Such a charge transfer is expected to shorten the Fe-O distance and consequently reduce the volume of FeO_6 octahedra, which should cause both iron polyhedra and the entire structure to become highly incompressible. Indeed, fitting the experimental SC-XRD pressure-volume data for cubic FeO_2 with the 3rd order Birch-Murnaghan equation of state (EoS) gave the EoS parameters with a large bulk modulus: $V_0 = 97.6(3) \text{ \AA}^3$, the unit cell volume; $K_0 = 305(9)$ GPa, the bulk modulus; and $K' = 4.0$ (fixed), the pressure derivative of the bulk modulus. The compressibility of FeO_6 octahedra is low ($K_{0,\text{octa.}} = 350(4)$ GPa) and the octahedral volume is significantly smaller than that known for any other compound, including those with ferric iron in the low-spin state (Fig. 1(b)).

We complimented studies of cubic FeO_2 by investigations of high-pressure behavior of iron (III) oxyhydroxide, FeO_2H_x . Laser heating of goethite, $\alpha\text{-FeOOH}$, at $\sim 81(2)$ GPa and 1500(100) K resulted in formation of a cubic phase with the lattice parameter $a = 4.430(1)$ \AA . The structure was solved and refined from SC-XRD data (Table S2[6]), and the arrangement of Fe and O was found to correspond to the HP-PdF₂-type structure, confirming that FeO_2 and FeO_2H_x are isostructural phases. The lattice parameter suggests the chemical composition $\text{FeO}_2\text{H}_{0.4}$ [37]. The relatively high value of the shortest O-O distance ($\sim 2.262(5)$ \AA) rules out the peroxide-type chemical bonding between oxygen atoms and the pres-

ence of hydrogen does not shorten this bond length.

In order to confirm the oxidation state of iron in cubic FeO_2H_x , we performed *in situ* XANES measurements on the sample synthesized by laser heating of goethite at 86(2) GPa and 1700(200) K in a DAC equipped with anvils made of polycrystalline diamonds [38]. Powder XRD data confirmed the synthesis of material with the lattice parameter $a = 4.449(5)$ Å (Fig. S5), which corresponds to the composition $\text{FeO}_2\text{H}_{0.5}$. In the XANES spectra collected in the center of a sample at the Fe K_α edge, the pre-edge peak narrows after synthesis of $\text{FeO}_2\text{H}_{0.5}$, and a negligible changes in the edge feature are observed; however, the position of the absorption jump remains the same for the starting FeOOH and cubic $\text{FeO}_2\text{H}_{0.5}$ (Fig. 4), inferring that iron does not alter its oxidation state during this transformation and remains 3+. We have performed the XANES mapping of a whole sample with 3 μm step to verify the sample homogeneity. The comparative contrast maps [42] were built for different energy Regions of Interest (ROI) (~ 7121 eV [ROI 1], ~ 7124 eV [ROI 2] and ~ 7131 eV [ROI 3] corresponding to the beginning of the edge, edge feature and the normalized first XANES peak correspondingly, see Fig. 5). The contrast built for the [ROI 2]:[ROI 3] suggest small deviations of a XANES edge feature caused by the presence of negligible amount of FeOOH on the edges of a sample (the spectrum collected at point 2 in Fig. 5) due to the temperature gradients during laser heating. In the same time, [ROI 1]:[ROI 3] contrast map, sensitive to the position of the edge, rules out the presence of Fe^{2+} in the sample. Comparison of XANES data obtained from the starting FeOOH and $\text{FeO}_2\text{H}_{0.5}$ and the contrast maps unambiguously confirms that iron is ferric in both species (Figs. 4 and 5). Therefore, oxygen in $\text{FeO}_2\text{H}_{0.5}$ has the formal oxidation state 1.75–.

Generalizing our observations on cubic HP-PdF₂-structured FeO_2 and FeO_2H_x phases and taking into account that compounds with x up to 1 have been described in the literature, we conclude that at pressures above ~ 50 GPa, the oxidation state of oxygen can significantly deviate from 2–. Experimental and theoretical results on cubic FeO_2 and FeO_2H_x phases may be concise in terms of the concept of valence. For our purposes we accept a definition of the “valence” of an element as a measure of its combining power with other atoms when it forms chemical compounds, or, as in the bond valence model [39], as the number of electrons the atom uses for bonding. Thus, in the HP-PdF₂-type structured FeO_2 and $\text{FeO}_2\text{H}_{0.5}$ iron has the valence 3+, and oxygen – 1.5 and 1.75, correspondingly. Reducing the oxygen valence from 2, common for oxides, down to 1.5 can be explained by a formation of a localized hole at oxygen sites, which leads to a reduction of the Fe-O distance and, as a consequence, of the volume of FeO_6 octahedra.

In conclusions, our results show that iron (III) dioxide FeO_2 can form at ~ 45 GPa, i.e., at significantly milder

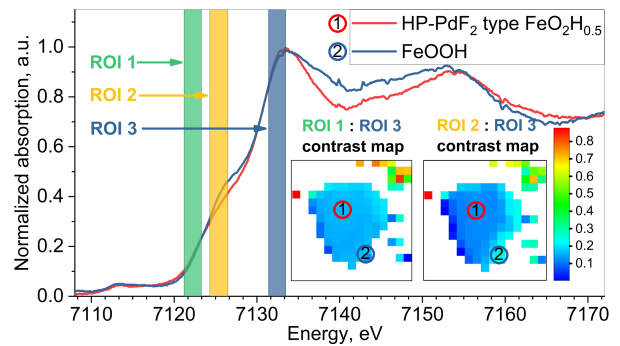


FIG. 5: (Color online) Fe K_α edge XAS spectra and contrast maps of starting FeOOH and $\text{FeO}_2\text{H}_{0.5}$ synthesized by laser heating to 1700(200) K at 86(2) GPa (DAC11, see Table S1). XAS spectra collected at different spots of the sample are denoted by red and blue circles with numbers (red line and point 1 corresponds to the cubic $\text{FeO}_2\text{H}_{0.5}$ and blue line and point 2 corresponds to the remaining FeOOH). The inset shows the contrast maps built for different ROIs (each pixel of the map corresponds to the spectra collected with 3 μm steps over the sample chamber). The ranges of ROIs used to build contrast maps described in [42] are highlighted in colors.

conditions than reported earlier (~ 75 GPa) [7], which corresponds to the pressures at the depth of ~ 1150 km in the upper part of the Earth’s lower mantle. However, the high oxidation state of iron in HP-PdF₂-type cubic FeO_2 and FeO_2H_x phases makes their appearance hardly possible for any plausible equilibrium homogeneous lower mantle assemblages with the oxygen fugacity below iron-wüstite buffer [40].

The authors acknowledge the Deutsches Elektronen-Synchrotron (DESY, PETRA III), the European Synchrotron Radiation Facility (ESRF), and the Advance Photon Source (APS) for provision of beamtime. N.D. and L.D. thank the Federal Ministry of Education and Research, Germany (BMBF, grant no. 05K19WC1) and the Deutsche Forschungsgemeinschaft (DFG projects DU 954-11/1, DU 393-9/2, and DU 393-13/1) for financial support. N.D. thanks the Swedish Government Strategic Research Area in Materials Science on Functional Materials at Linköping University (Faculty Grant SFO-Mat-LiU No. 2009 00971). Electronic structure calculations were supported by the Russian Science Foundation (Project No. 18-12-00492). Theoretical analysis of chemical bonding was supported by the Ministry of Science and Higher Education of the Russian Federation in the framework of Increase Competitiveness Program of NUST “MISIS” (No. K2-2019-001) implemented by a governmental decree dated 16 March 2013, No. 211. Support from the Knut and Alice Wallenberg Foundation (Wallenberg Scholar Grant No. KAW-2018.0194), the Swedish Government Strategic Research Areas in Materials Science on Functional Materials at Linköping University (Faculty Grant SFO-Mat-LiU No. 2009 00971) and SeRC, and the

Swedish Research Council (VR) grant No. 2019-05600 is gratefully acknowledged.

-
- [1] A. B. Woodland, J. Kornprobst, and A. Tabit, Ferric Iron in Orogenic Lherzolite Massifs and Controls of Oxygen Fugacity in the Upper Mantle, *Lithos* **89**, 222 (2006).
- [2] B. Lavina and Y. Meng, Unraveling the Complexity of Iron Oxides at High Pressure and Temperature: Synthesis of Fe_5O_6 , *Sci. Adv.* **1**, e1400260 (2015).
- [3] E. Bykova, L. Dubrovinsky, N. Dubrovinskaia, M. Bykov, C. McCammon, S. V. Ovsyannikov, H.-P. Liermann, I. Kuppenko, A. I. Chumakov, R. Ruffer, M. Hanfland, and V. Prakapenka, Structural Complexity of Simple Fe_2O_3 at High Pressures and Temperatures, *Nat. Commun.* **7**, 10661 (2016).
- [4] S. V. Ovsyannikov, M. Bykov, E. Bykova, K. Glazyrin, R. S. Manna, A. A. Tsirlin, V. Cerantola, I. Kuppenko, A. V. Kurnosov, I. Kantor, A. S. Pakhomova, I. Chuvashova, A. I. Chumakov, R. Ruffer, C. McCammon, and L. S. Dubrovinsky, Pressure Tuning of Charge Ordering in Iron Oxide, *Nat. Commun.* **9**, 4142 (2018).
- [5] R. Sinmyo, E. Bykova, S. V. Ovsyannikov, C. McCammon, I. Kuppenko, L. Ismailova, and L. Dubrovinsky, Discovery of Fe_7O_9 : A New Iron Oxide with a Complex Monoclinic Structure, *Sci. Rep.* **6**, 32852 (2016).
- [6] See Supplemental Material at for Additional Tables, Figures, Description of Methods, and Discussions.
- [7] Q. Hu, D. Y. Kim, W. Yang, L. Yang, Y. Meng, L. Zhang, and H. K. Mao, FeO_2 and FeOOH under Deep Lower-Mantle Conditions and Earth's Oxygen-Hydrogen Cycles, *Nature* **534**, 241 (2016).
- [8] Q. Hu and J. Liu, Deep Mantle Hydrogen in the Pyrite-Type FeO_2 - FeO_2H System, *Geosci. Front.*, <https://doi.org/10.1016/j.gsf.2020.04.006> (2020).
- [9] M. Nishi, Y. Kuwayama, J. Tsuchiya, and T. Tsuchiya, The Pyrite-Type High-Pressure Form of FeOOH , *Nature* **547**, 205 (2017).
- [10] E. Boulard, M. Harmand, F. Guyot, G. Lelong, G. Morard, D. Cabaret, S. Boccato, A. D. Rosa, R. Briggs, S. Pascarelli, and G. Fiquet, Ferrous Iron under Oxygen-Rich Conditions in the Deep Mantle, *Geophys. Res. Lett.* **46**, 1348 (2019).
- [11] J. Liu, Q. Hu, W. Bi, L. Yang, Y. Xiao, P. Chow, Y. Meng, V. B. Prakapenka, H. K. Mao, and W. L. Mao, Altered Chemistry of Oxygen and Iron under Deep Earth Conditions, *Nat. Commun.* **10**, 153 (2019).
- [12] B. G. Jang, D. Y. Kim, and J. H. Shim, Metal-Insulator Transition and the Role of Electron Correlation in FeO_2 , *Phys. Rev. B* **95**, 075144 (2017).
- [13] B. G. Jang, J. Liu, Q. Hu, K. Haule, H. K. Mao, W. L. Mao, D. Y. Kim, and J. H. Shim, Electronic Spin Transition in FeO_2 : Evidence for Fe(II) with Peroxide O_2^{2-} , *Phys. Rev. B* **100**, 014418 (2019).
- [14] E. Koemets, L. Yuan, E. Bykova, K. Glazyrin, E. Ohtani, and L. Dubrovinsky, Interaction between FeOOH and NaCl at Extreme Conditions: Synthesis of Novel $\text{Na}_2\text{FeCl}_4\text{OH}_x$ Compound, *Minerals* **10**, 51 (2020).
- [15] E. Bykova, Single-Crystal X-Ray Diffraction at Extreme Conditions in Mineral Physics and Material Sciences, Thesis. Bayreuther Graduiertenschule Für Math. Und Naturwissenschaften. 282 (2015).
- [16] S. S. Streltsov, A. O. Shorikov, S. L. Skornyakov, A. I. Poteryaev, and D. I. Khomskii, Unexpected 3+ Valence of Iron in FeO_2 , a Geologically Important Material Lying “in between” Oxides and Peroxides, *Sci. Rep.* **7**, 13005 (2017).
- [17] A. O. Shorikov and S. V. Streltsov, Equation of State of FeO_2 , *J. Magn. Magn. Mater.* **459**, 280 (2017).
- [18] A. T. Garcia-Sosa and M. Castro, Density Functional Study of FeO_2 , FeO_2^+ , and FeO_2^- , *Int. J. Quantum Chem.* **80**, 307 (2000).
- [19] C. Lu, M. Amsler, and C. Chen, Unraveling the Structure and Bonding Evolution of the Newly Discovered Iron Oxide FeO_2 , *Phys. Rev. B* **98**, 054102 (2018).
- [20] A. Georges, G. Kotliar, W. Krauth, and M. Rozenberg, Dynamical Mean-Field Theory of Strongly Correlated Fermion Systems and the Limit of Infinite Dimensions, *Rev. Mod. Phys.* **68**, 13 (1996).
- [21] L. V. Pourovskii, B. Amadon, S. Biermann, and A. Georges, Self-Consistency over the Charge Density in Dynamical Mean-Field Theory: A Linear Muffin-Tin Implementation and Some Physical Implications, *Phys. Rev. B* **76**, 235101 (2007).
- [22] I. Leonov, Metal-Insulator Transition and Local-Moment Collapse in FeO under Pressure, *Phys. Rev. B* **92**, 085142 (2015).
- [23] I. Leonov, L. Pourovskii, A. Georges, and I. A. Abrikosov, Magnetic Collapse and the Behavior of Transition Metal Oxides at High Pressure, *Phys. Rev. B* **94**, 155135 (2016).
- [24] E. Greenberg, R. Nazarov, A. Landa, J. Ying, R. Q. Hood, B. Hen, R. Jeanloz, V. B. Prakapenka, V. V. Struzhkin, G. Kh. Rozenberg, I. Leonov, Phase transitions and spin-state of iron in FeO at the conditions of Earth's deep interior, arXiv:2004.00652 (2020).
- [25] S. L. Skornyakov, V. I. Anisimov, D. Vollhardt, and I. Leonov, Effect of electron correlations on the electronic structure and phase stability of FeSe upon lattice expansion, *Phys. Rev. B* **96**, 035137 (2017); S. L. Skornyakov, V. I. Anisimov, D. Vollhardt, and I. Leonov, Correlation strength, Lifshitz transition, and the emergence of a two-dimensional to three-dimensional crossover in FeSe under pressure, *Phys. Rev. B* **97**, 115165 (2018).
- [26] E. Greenberg, I. Leonov, S. Layek, Z. Konopkova, M. P. Pasternak, L. Dubrovinsky, R. Jeanloz, I. A. Abrikosov, and G. K. Rozenberg, Pressure-Induced Site-Selective Mott Insulator-Metal Transition in Fe_2O_3 , *Phys. Rev. X* **8**, 031059 (2018).
- [27] I. Leonov, G. K. Rozenberg, and I. A. Abrikosov, Charge Disproportionation and Site-Selective Local Magnetic Moments in the Post-Perovskite-Type Fe_2O_3 under Ultra-High Pressures, *npj Comput. Mater.* **5**, 90 (2019).
- [28] I. Leonov, A. O. Shorikov, V. I. Anisimov, and I. A. Abrikosov, Emergence of Quantum Critical Charge and Spin-State Fluctuations near the Pressure-Induced Mott Transition in MnO , FeO , CoO , and NiO , *Phys. Rev. B* **101**, 245144 (2020).
- [29] E. Ito, H. Fukui, T. Katsura, D. Yamazaki, T. Yoshino, Y. I. Aizawa, A. Kubo, S. Yokoshi, K. Kawabe, S. Zhai, A. Shatzkiy, M. Okube, A. Nozawa, and K. I. Funakoshi, Determination of High-Pressure Phase Equilibria of Fe_2O_3 Using the Kawai-Type Apparatus Equipped with Sintered Diamond Anvils, *Am. Mineral.* **94**, 205 (2009).
- [30] W.-K. Li, G.-D. Zhou, and T. C. W. Mak, *Advanced*

- Structural Inorganic Chemistry, Vol. 10 (Oxford University Press, 2008).
- [31] J. Haines, J. M. Leger, M. W. Schmidt, J. P. Petitet, a S. Pereira, J. a H. Da Jornada, and S. Hull, Structural Characterization of the $Pa\bar{3}$ -Type, High Pressure Phase of Ruthenium Dioxide, *J. Phys. Chem. Solids* **59**, 239 (1998).
- [32] Y. Shirako, X. Wang, Y. Tsujimoto, K. Tanaka, Y. Guo, Y. Matsushita, Y. Nemoto, Y. Katsuya, Y. Shi, D. Mori, H. Kojitani, K. Yamaura, Y. Inaguma, and M. Akaogi, Synthesis, Crystal Structure, and Electronic Properties of High-Pressure PdF₂-Type Oxides MO₂ ($M = Ru, Rh, Os, Ir, Pt$), *Inorg. Chem.* **2**, 11616 (2014).
- [33] C. T. Prewitt and R. T. Downs, Chapter 9 High-pressure crystal chemistry, *Rev. Mineral. Geochemistry* **37**, 283 (1998).
- [34] J. Zaanen, G. A. Sawatzky, and J. W. Allen, Band Gaps and Electronic Structure of Transition-Metal Compounds, *Phys. Rev. Lett.* **55**, 418 (1985).
- [35] M. A. Korotin, V. I. Anisimov, D. I. Khomskii, G. A. Sawatzky, CrO₂: A Self-Doped Double Exchange Ferromagnet, *Phys. Rev. Lett.* **80**, 4305 (1998).
- [36] P. Gütllich, E. Bill, and A. X. Trautwein, Mössbauer Spectroscopy and Transition Metal Chemistry, *Climate Change 2013 - The Physical Science Basis*.
- [37] Q. Hu, D. Y. Kim, J. Liu, Y. Meng, L. Yang, D. Zhang, W. L. Mao, and H. Mao, Dehydrogenation of Goethite in Earth's Deep Lower Mantle, *Proc. Natl. Acad. Sci.* **114**, 201620644 (2017).
- [38] N. Ishimatsu, K. Matsumoto, H. Maruyama, N. Kawamura, M. Mizumaki, H. Sumiya, and T. Irifune, Glitch-Free X-Ray Absorption Spectrum under High Pressure Obtained Using Nano-Polycrystalline Diamond Anvils, *J. Synchrotron Radiat.* **19**, 768 (2012).
- [39] I. D. Brown and K. R. Poeppelmeier, Editors. *Bond Valences*, Vol. 158.
- [40] D. J. Frost and C. A. McCammon, The Redox State of Earth's Mantle, *Annu. Rev. Earth Planet. Sci.* **36**, 389 (2008).
- [41] A. Kjekshus and T. Rakke, Preparations and Properties of Magnesium, Copper, Zinc, and Cadmium Dichalcogenides, *Acta Chem. Scand. Ser. A* **33**, 617 (1979).
- [42] G. Aprilis, I. Kantor, I. Kuppenko, V. Cerantola, A. Pakhomova, I. E. Collings, R. Torchio, T. Fedotenko, S. Chariton, M. Bykov, E. Bykova, E. Koemets, D. M. Vasiukov, C. McCammon, L. Dubrovinsky, and N. Dubrovinskaia, Comparative Study of the Influence of Pulsed and Continuous Wave Laser Heating on the Mobilization of Carbon and Its Chemical Reaction with Iron in a Diamond Anvil Cell, *J. Appl. Phys.* **125**, 095901 (2019).
- [43] D. M. Vasiukov, L. Dubrovinsky, I. Kuppenko, V. Cerantola, G. Aprilis, L. Ismailova, E. Bykova, C. McCammon, C. Prescher, A. I. Chumakov, and N. Dubrovinskaia, Pressure-Induced Spin Pairing Transition of Fe³⁺ in Oxygen Octahedra, arXiv:1710.03192 (2017).
- [44] I. Kantor, V. Prakapenka, A. Kantor, P. Dera, A. Kurnosov, S. Sinogeikin, N. Dubrovinskaia, and L. Dubrovinsky, BX90: A New Diamond Anvil Cell Design for X-Ray Diffraction and Optical Measurements, *Rev. Sci. Instrum.* **83**, 125102 (2012).
- [45] M. Merlini and M. Hanfland, Single-Crystal Diffraction at Megabar Conditions by Synchrotron Radiation, *High Press. Res.* **33**, 511 (2013).
- [46] H. P. Liermann, Z. Konopková, W. Morgenroth, K. Glazyrin, J. Bednarčík, E. E. McBride, S. Petitgirard, J. T. Delitz, M. Wendt, Y. Bican, A. Elnes, I. Schwark, A. Rothkirch, M. Tischer, J. Heuer, H. Schulte-Schrepping, T. Kracht, and H. Franz, The Extreme Conditions Beamline P02.2 and the Extreme Conditions Science Infrastructure at PETRA III, *J. Synchrotron Radiat.* **22**, 908 (2015).
- [47] C. Prescher and V. B. Prakapenka, DIOPTAS: A Program for Reduction of Two-Dimensional X-Ray Diffraction Data and Data Exploration, *High Press. Res.* **35**, 223 (2015).
- [48] C. Prescher, C. McCammon, and L. Dubrovinsky, MossA: A Program for Analyzing Energy-Domain Mössbauer Spectra from Conventional and Synchrotron Sources, *J. Appl. Crystallogr.* **45**, 329 (2012).
- [49] G. M. Sheldrick, Crystal Structure Refinement with SHELXL, *Acta Crystallogr. Sect. C Struct. Chem.* **71**, 3 (2015).
- [50] K. Momma and F. Izumi, VESTA 3 for Three-Dimensional Visualization of Crystal, Volumetric and Morphology Data, *J. Appl. Crystallogr.* **44**, 1272 (2011).
- [51] I. Leonov, V. I. Anisimov, and D. Vollhardt, Metal-Insulator Transition and Lattice Instability of Paramagnetic V₂O₃, *Phys. Rev. B* **91**, 195115 (2015).
- [52] G. Trimarchi, I. Leonov, N. Binggeli, D. Korotin, and V. I. Anisimov, LDA+DMFT Implemented with the Pseudopotential Plane-Wave Approach, *J. Phys. Condens. Matter* **20**, 135227 (2008).
- [53] E. Gull, A. J. Millis, A. I. Lichtenstein, A. N. Rubtsov, M. Troyer, and P. Werner, Continuous-Time Monte Carlo Methods for Quantum Impurity Models, *Rev. Mod. Phys.* **83**, 349 (2011).
- [54] G. Kresse and J. Furthmüller, Efficiency of Ab-Initio Total Energy Calculations for Metals and Semiconductors Using a Plane-Wave Basis Set, *Comput. Mater. Sci.* **6**, 15 (1996).
- [55] D. Joubert, From Ultrasoft Pseudopotentials to the Projector Augmented-Wave Method, *Phys. Rev. B* **9**, 1758 (1999).
- [56] G. Kresse and J. Furthmüller, Efficient Iterative Schemes for Ab Initio Total-Energy Calculations Using a Plane-Wave Basis Set, *Phys. Rev. B* **54**, 11169 (1996).
- [57] J. Heyd, G. E. Scuseria, and M. Ernzerhof, Hybrid Functionals Based on a Screened Coulomb Potential, *J. Chem. Phys.* **118**, 8207 (2003).